95-282

E3-95-282

Al.Yu.Muzychka, Yu.N.Pokotilovski

MONTE CARLO SIMULATION OF SPECTRAL FILTERS FOR ULTRACOLD NEUTRONS

1995

1 Introduction

The spectra of neutrons, emerging from neutron guides transporting UCN from moderators to experimental installations, usually contain a significant admixture of neutrons with higher energies. This surplus of more energetic neutrons often surpasses the flux of UCN by many times. Fig.1 shows the neutron spectra from UCN channels of the ILL High Flux Reactor (Steyerl turbine)[1] and the Gatchina reactor of St.Petersburg Nuclear Physics Institute[2]. For some important experiments based on UCN storage in closed chambers for long periods of time – tens or hundreds of seconds (e.g. neutron EDM searches or neutron lifetime measurements – see for example the recent review in[3] and references therein) the presence of these more energetic neutrons in the storage volume is not a serious hindrance to the experiment. During a comparatively short time – several seconds – these neutrons, having accessible angles for penetrating the chamber wall, are captured or upscattered inside the wall and generally do not influence the results of the measurement.

But there are some cases in which the presence of neutrons with energies higher than some strictly determined critical energy (super-barrier neutrons) is detrimental to the correct interpretation of the experiment. The most interesting are experiments connected with the long standing puzzle of anomalous losses of UCN at their interaction with a solid reflecting surface. The problem consists of a two to three orders of magnitude discrepancy between the theoretical value of the UCN loss coefficient, based on a simple quantum mechanical model of interaction of the neutron wave with a reflecting wall, and the experimental one (e.g. for beryllium and solid oxygen, this experimental loss coefficient has a value $\eta \approx (2-3) \cdot 10^{-5}$[4, 5]). This anomalously high experimental loss coefficient, which surprisingly weakly changes with surface temperature, may be caused by some unknown additional loss process occuring at the wall surface.

In the experimental investigation of anomalous UCN upscattering at their reflection from a solid surface[4, 6] as a possible reason of UCN loss, it is important to be confident that the measured flux of upscattered neutrons is not caused by the upscattering of UCN with energies larger than the boundary energy of the reflecting surface, and which penetrate deeply into the bulk of the wall substance. The same applies to

2

experiments searching for the anomalous propagation of sub-barrier UCN deep into the reflecting wall, e.g., by the method of activation[7] or by the method of measuring the anomalous UCN flux propagating through foils[5]. In both of these cases super-barrier neutrons might imitate the searched for effect. For example a 1% admixture of the super-barrier neutrons with energies surpassing the boundary energy by 1% percent gives, at the isotropic angular distribution of incoming neutrons, a penetration probability into the bulk as high as $1 \cdot 10^{-4}$. Other possible future applications of irradiation of a surface with UCN flux with the aim, e.g., of neutron surface activation analysis or measurement of the frequency spectrum of a surface or of adsorbed atoms, may encounter similarly stringent requirements on the level of admixture super-barrier neutrons.

Over the years, different devices have been used for preliminary preparation of the UCN spectrum before allowing neutrons to enter the experimental chambers. The task of such devices was to restrict, as much as possible, the access of UCN with energies higher than some critical energy into the chamber and to let UCN with lower energies pass with the smallest losses. The general idea of such devices consists in arranging some kind of geometric trap for UCN, in which the more energetic neutrons will "die out" at a higher rate due to their larger probability of penetrating the bulk and being captured in the wall. No quantitative analysis of the merits and demerits of different kinds of such devices, however, has been published. In this paper we want to present the results of a Monte Carlo simulation of UCN transport through several types of these devices.

2   Monte Carlo simulation

The geometric types of UCN spectral filters investigated in our simulation are shown in fig.2. The device of fig.1a is a cylindrical or rectangular (in our calculations) vessel, in which UCN have to experience (on the average) a significant quantity of reflections before leaving the vessel through the exit window. In the device of fig. 2a, the entrance and exit inner guides have lengths equal to or larger than half the length of the box.

The fig.2b filter consists of a segment of straight neutron guide with a sequence of partitions, and in the device of fig.2c these partitions are

3
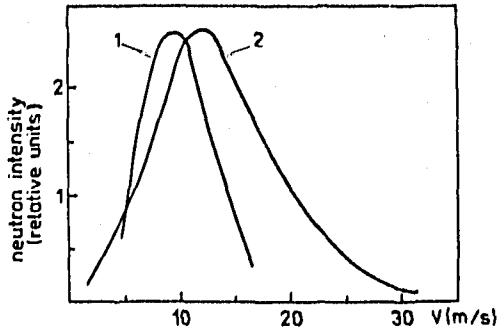
Fig.1 The very cold and ultracold neutron spectra measured at the exits of: 1 - ILL (Grenoble) ultracold neutron source (Steyerl turbine) [1], 2 - vertical channel of SPNPI Gatchina reactor[2]. The spectra are not shown to scale; in reality the ILL intensity is about an order of magnitude higher.
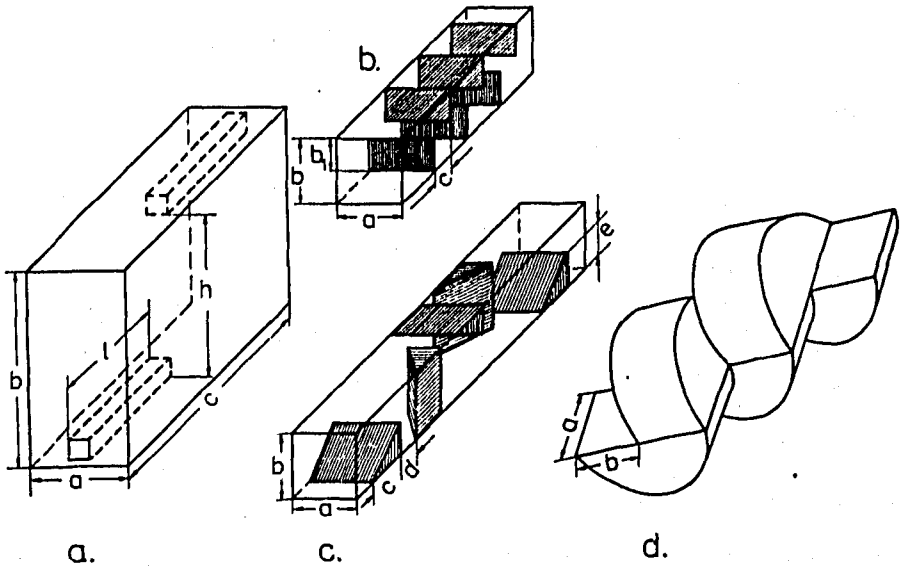
Fig.2 Configurations of the UCN spectral filters used in the Monte Carlo simulations: a–rectangular storage volume with inner neutron guides, b–segment of a straight neutron guide with plane partitions, c– the same with truncated partitions, d–periodic structure of short half-cylinder neutron guides.

4

truncated. The device of fig.2d consists of half-cylindrical tubes, connected to each other in such a way that any neutron passing through the sequence of such tubes will, with large probability, experience collisions with the guide's surface at an angle close to normal.

The filters of types 2a and 2b were used previously in different UCN groups, without a careful analysis of their properties however; the filters of fig.2c and 2d are considered here for the first time.

In all calculations the incoming UCN angular distribution has the form:

$$dw(\theta) \sim cos\theta \cdot d\Omega, \tag{1}$$

where θ is the UCN momentum polar angle relative to the axis normal to the entrance window of the device.

The angular distribution of UCN elastically reflected from the surface was supposed to consist of two parts: specular and diffuse. For the case of a rough surface we used a simple model of diffuse reflection in which the angular distribution has the form:

$$dw_{d.r.} = \Delta \cdot cos\theta \cdot d\Omega, \tag{2}$$

where θ is the scattering angle with respect to the surface normal and Δ is the probability of diffuse scattering. The distribution (2) may approximately correspond to a very macroscopically rough surface when the reflection angle does not depend on wave length or incident angle of the neutron (except at small grazing angles, when the reflected intensity is not symmetrical with respect to the surface normal).

The case of a smooth surface corresponds to the angular distribution of reflected neutrons derived in [8], in which the neutron momentum transfer dependence of the diffuse reflection probability has the form:

$$w_{d.r.}(\Omega_0, \Omega) = \frac{k_b^4}{4cos\theta_0} \cdot |S(\theta_0)|^2 \cdot |S(\theta)|^2 \cdot F(\mu), \tag{3}$$

for the diffuse neutron scattering away from the wall, and

$$w_{d.r.}(\Omega_0, \Omega) = \frac{k_b^4}{4cos\theta_0} \frac{k'}{k} \cdot |S(\theta_0)|^2 \cdot |S'(\theta')|^2 \cdot F(\mu),$$
$$\text{for} \quad cos^2(\theta') \cdot k'^2 > -k_b^2$$
$$w_{d.r.}(\Omega_0, \Omega) = 0, \quad \text{for} \quad cos^2(\theta') \cdot k'^2 < -k_b^2. \tag{4}$$

for the diffuse neutron scattering into the wall.

$$S(\theta) = \frac{2\cos\theta}{\cos\theta + (\cos^2\theta - k_b^2/k^2)^{1/2}}, \tag{5}$$

$$S'(\theta') = \frac{2\cos\theta'}{\cos\theta' + (\cos^2\theta' + k_b^2/k'^2)^{1/2}}, \tag{6}$$

In these expressions k is the wave vector of the incident (and reflected away from the wall) neutrons, k' is the wave vector of the diffusively scattered neutron inside the wall characterized by the boundary wave vector k_b.

$$F(\mu) = \sigma^2 T^2/2\pi \cdot exp(-\mu^2 T^2/2), \tag{7}$$

$$\mu^2 = (\vec{k}_{||} - \vec{k}_{||0})^2, \tag{8}$$

$\vec{k}_{||0}$ and $\vec{k}_{||}$ are the parallel to the surface plane components of incident and scattered wave vectors, so that

$$(\vec{k}_{||} - \vec{k}_{||0})^2 = k^2(sin^2\theta_0 + sin^2\theta - 2sin\theta \cdot sin\theta_0 \cdot cos(\phi - \phi_0)). \tag{9}$$

Here θ_0 and θ, ϕ_0 and ϕ are the polar and azimuth angles of the incident to the surface normal and reflected neutrons, respectively; σ and T in (7) are surface roughness parameters for random deviations of the surface from ideal plane geometry which are described by an autocorrelation function:

$$f(\vec{\rho} - \vec{\rho}') = \sigma^2 \cdot exp(-(\vec{\rho} - \vec{\rho}')^2/2T^2). \tag{10}$$

Integrating (3) and (4) over Ω gives the total probability of diffuse reflection:

$$\Delta = \int w_{d.r.}(\Omega_0, \Omega)d\Omega. \tag{11}$$

For

$$\lambda = 2\pi/k \cong 600 \text{ Å } (v \cong 5m/s), \quad \sigma \cong 25 \text{ Å},$$
$$T \cong 500 \text{ Å}, \quad \theta_0 \cong \pi/4, \quad \Delta \cong 0.1. \tag{12}$$

The considered roughness parameters $\sigma = 25$Å, $T = 250$Å or 500Å are quite realistic [8, 9] for polished metal surfaces.

UCN loss due to capture and inelastic scattering are described by the expression:

$$\mu(v,\theta) = 2\eta \frac{v \cdot cos\theta}{v_b} \bigg/ \sqrt{1 - \left(\frac{v \cdot cos\theta}{v_b}\right)^2}. \tag{13}$$

Here θ is the incident angle to the surface normal, $\eta = Im\ b/Re\ b$, $Im\ b = (\sigma_c + \sigma_{in})/2\lambda$, σ_c and σ_{in} are the capture and the inelastic cross sections, respectively. In the calculations we took $\eta = 5 \cdot 10^{-4}$. This value is approximately twice as large if compared with the theoretical η for nickel or stainless steel.

Neutrons with energies higher than the boundary energy of the internal surface material of the device also have the possibility to penetrate the bulk material – **the main phenomenon with which the filtering process works**. The neutron reflection probability in this case has the form:

$$R = \left|\left(v_\perp - \sqrt{v_\perp^2 - v_0^2}\right) \bigg/ \left(v_\perp + \sqrt{v_\perp^2 - v_0^2}\right)\right|^2, \tag{14}$$

where $v_\perp$ stands for the normal component of the neutron incoming velocity, and v_0 is the boundary velocity of the surface.

The boundary energy of the **internal surface of all UCN filters**, considered in these calculations is $E_{bf} = 204 neV$, $v_b = 6.3 m/s$, which corresponds to stainless steel properties – the most practical material. But when there is a need to irradiate surfaces with a boundary energy lower than the E_b for stainless steel, it is necessary to use additional neutron guide elements for connecting the irradiation chamber on a higher level with respect to the filter.

In all calculations gravity, which bends the neutron trajectories inside the filters, was rigorously taken into account.

3 Results of calculations

All calculations are based on not less than 2,000 histories for each incoming UCN velocity case for calculation of the UCN passage probability (up to 200 million histories in some cases).

Some results of calculations are shown in figs.3-17, which show the probability of UCN passing through a filter as a function of neutron energy for different devices. Figs.3 and 4 show the influence of inner
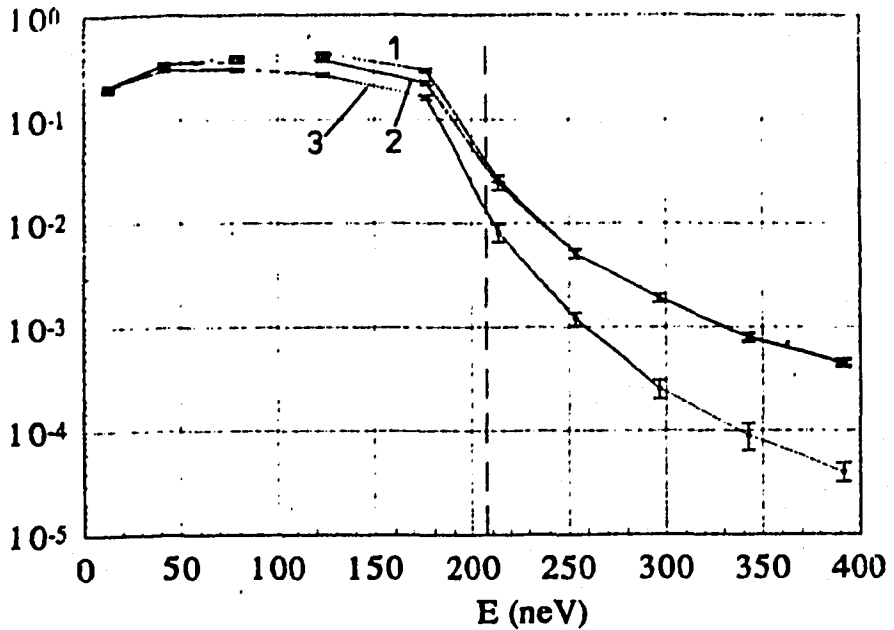
Fig.3 Energy dependence of neutron transmission through the filtering configuration of fig.2a, with dimensions: $a = b = 40cm$, $c = 100cm$, $l = 50cm$, $h = 30cm$, internal guides cross section is $6 \times 6cm^2$.

1. loss-less reflection inside the filter volume according to eq. (2) with $\Delta = 1.$; inner (length $l = 50cm$) neutron guides are perfectly mirror-like.

2. the same for a neutron loss coefficient at the inside surface of $\eta = 5 \cdot 10^{-4}$.

3. the same as 2) but the inside neutron guides have a reflection law according to eq.(3), with $\sigma = 30\text{Å}$, $T = 250\text{Å}$.
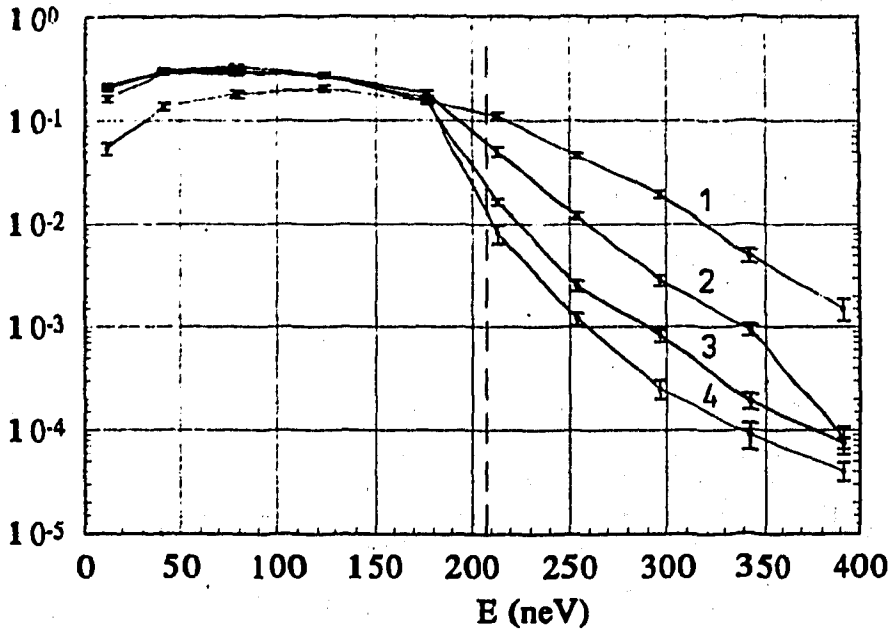
Fig.4 Energy dependence of neutron transmission through the filtering configuration of fig.2a, with dimensions: $a = b = 40cm$, $c = 100cm$, neutron loss coefficient of the inside surface $\eta = 5 \cdot 10^{-4}$, inner neutron guides with a length $l = 50cm$ have a reflection law according to eq. (3) with $\sigma = 30\text{Å}$, $T = 250\text{Å}$; the inside surface has a reflection law according to eq. (2):

1. $\Delta = 0$

2. $\Delta = 0.05$

3. $\Delta = 0.25$

4. $\Delta = 1$
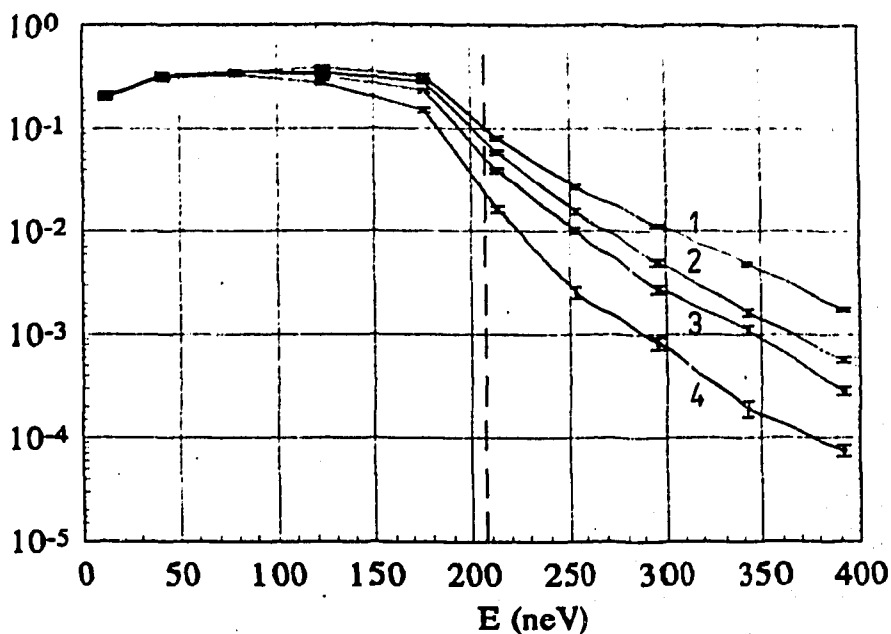
Fig.5 Energy dependence of neutron transmission through the filtering configuration of fig.2a with different dimensions, neutron loss coefficient of the inside surface $\eta = 5 \cdot 10^{-4}$, inner neutron guides with a length $l = c/2$ have a reflection law according to eq. (3) with $\sigma = 30\text{Å}$, $T = 250\text{Å}$; the inside surface has a reflection law according to eq. (2) with $\Delta = 0.25$.

1. $a = 50$, $b = 40cm$, $c = 15cm$.

2. $a = 15cm$, $b = 40cm$, $c = 50cm$.

3. $a = b = 40cm$, $c = 50cm$.

4. $a = b = 40cm$, $c = 100cm$.
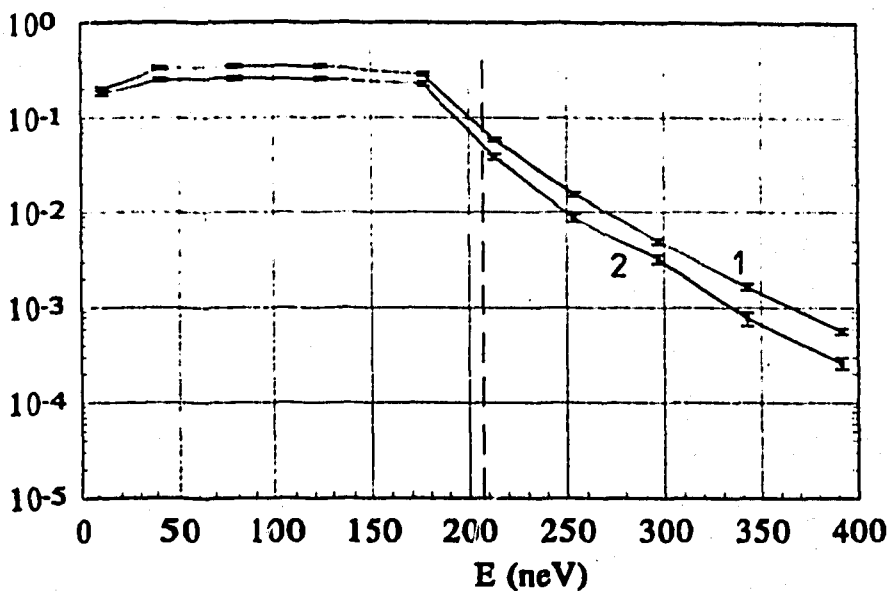
Fig.6 Energy dependence of neutron transmission through the filtering configuration of fig.2a with dimensions $a = 15cm$, $b = 40cm$, $c = 50cm$, neutron loss coefficient of the inside surface $\eta = 5 \cdot 10^{-4}$, inner neutron guides have a reflection law according to eq. (3) with $\sigma = 30\text{Å}$, $T = 250\text{Å}$, the inside surface has a reflection law according to eq. (2) with $\Delta = 0.25$ for different lengths l of the inner tubes:

1. $l = 25cm$

2. $l = 45cm$
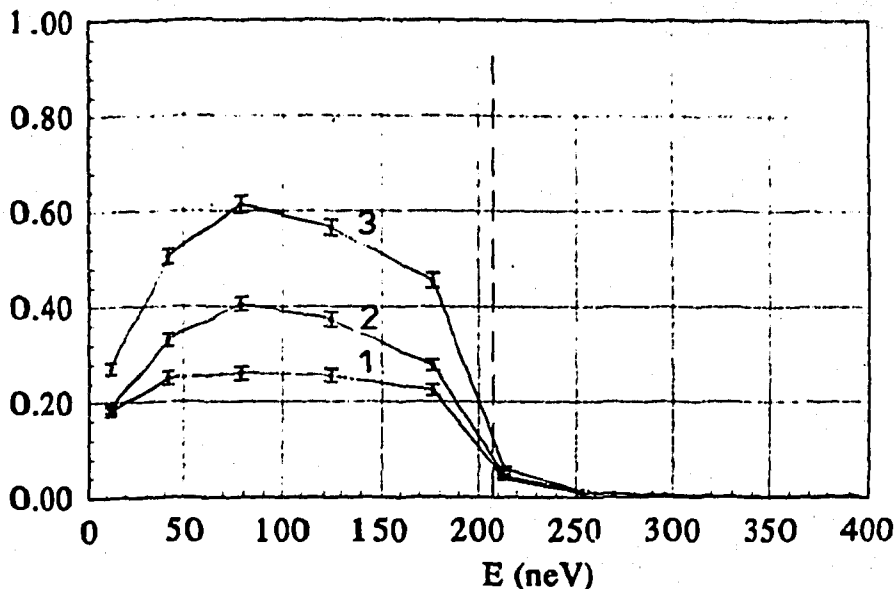
Fig.7 Energy dependence of neutron transmission through the filtering configuration of fig.2a, with dimensions $a = 15cm$, $b = 40cm$, $c = 50cm$, neutron loss coefficient of the inside surface $\eta = 5 \cdot 10^{-4}$, inner neutron guides with a length $l = 45cm$ have a reflection law according to eq. (3) with $\sigma = 30\text{Å}$, $T = 250\text{Å}$; the inside surface has a reflection law according to eq. (2) with $\Delta = 0.25$ for different probabilities α of UCN return from the exit window of the device:

1. $\alpha = 0$

2. $\alpha = 0.5$

3. $\alpha = 0.95$
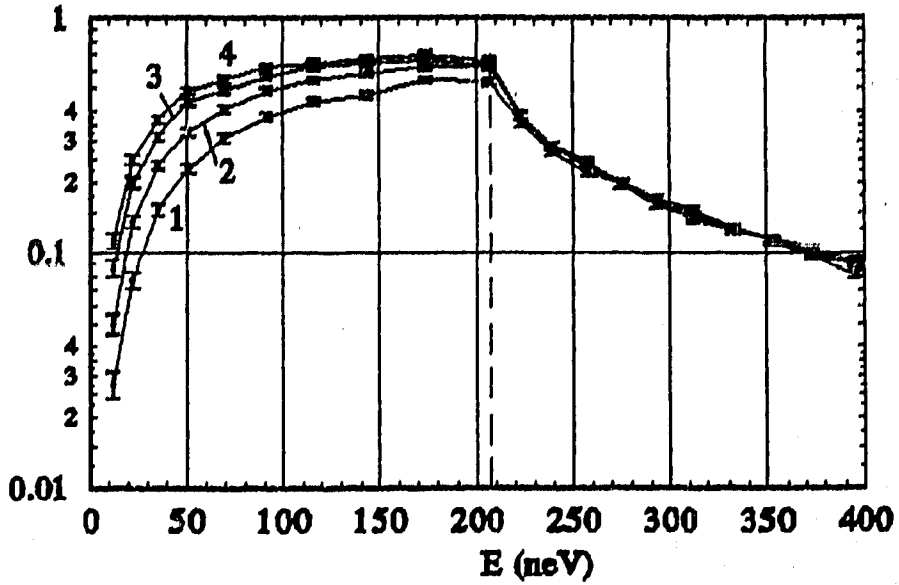
Fig.8 Energy dependence of the UCN return probability from a horizontal neutron guide with a cross section $6 \times 6 cm^2$, neutron surface reflection law according to eq. (3) with parameters $\sigma = 30\text{Å}$, $T = 250\text{Å}$.

1. guide length $3m$

2. guide length $6m$

3. guide length $12m$

4. guide length $18m$
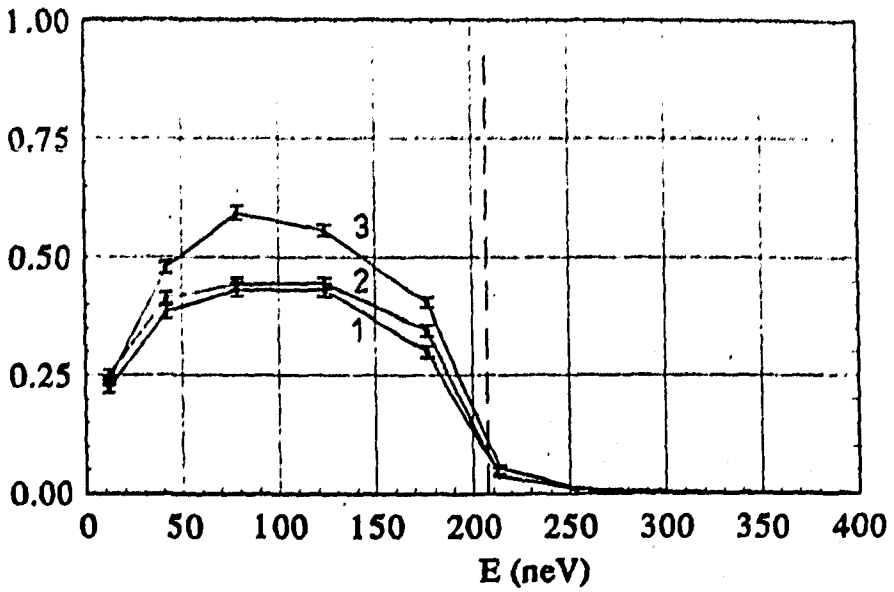
Fig.9 The same as in fig.7 but with a neutron guide 6m long at the entrance to the device. Its impact is the return of UCN to the entrance of the filter according to curve 1 of fig. 8.

14
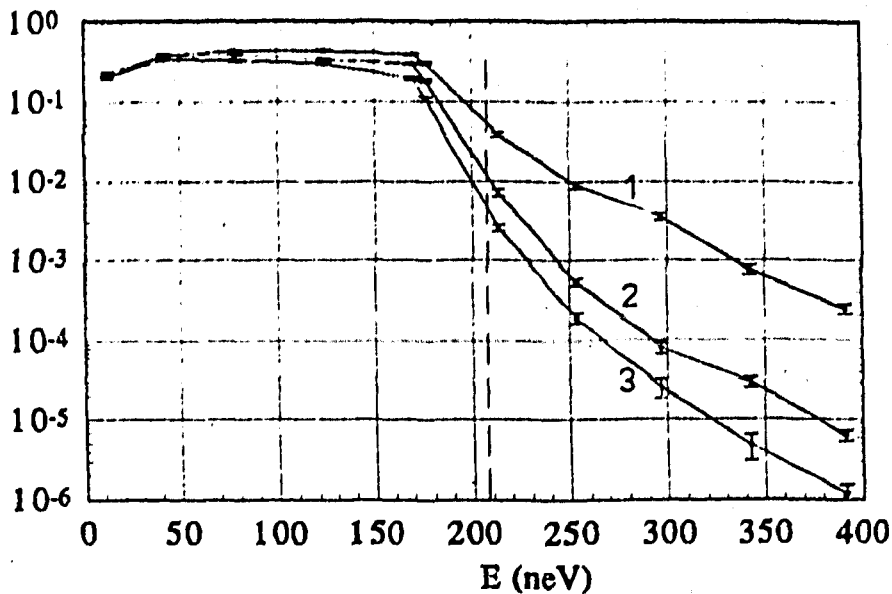
Fig.10 Energy dependence of neutron transmission through the filtering configuration of fig.2a, with dimensions $a = 15cm$, $b = 40cm$, $c = 50cm$, neutron loss coefficient of the inside surface $\eta = 5 \cdot 10^{-4}$; inner neutron guides with a length $l = 45cm$ have a reflection law according to eq. (3) with $\sigma = 30\text{Å}$, $T = 250\text{Å}$; the inside surface has a reflection law according to eq. (2) with $\Delta = 0.25$ for different rib densities on the inner surface of the device:

1. no ribs on the inner surface

2. ribs covering the inner surface, increasing its area 2.5 times

3. ribs covering the inner surface, increasing its area 5 times.
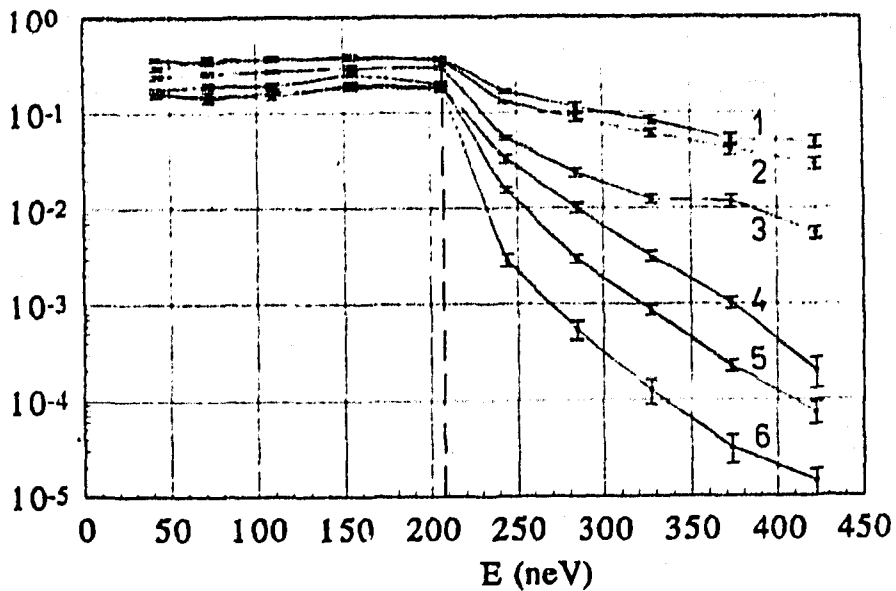
Fig.11 Energy dependence of neutron transmission through the filtering configuration of fig.2b, $a = b = 6cm$, $c = 3cm$, $b_1 = 3cm$, neutron loss coefficient of the inside surface $\eta = 5 \cdot 10^{-4}$, with different numbers of partitions and different degrees of inner surface roughness; the entrance of the filter is connected to the neutron guide with a cross section $6 \times 6cm^2$, length 6cm and neutron surface reflection law according to eq. (3) with parameters $\sigma = 30$ Å, $T = 250$Å; the exit of the filter is connected to the irradiation chamber with a return probability $\alpha = 0.5$

1. 3 partitions, mirror reflections

2. 6 partitions, mirror reflections

3. 3 partitions, reflection according eq. (2) with $\Delta = 0.25$

4. 6 partitions, reflection according eq. (2) with $\Delta = 0.25$

5. 3 partitions, reflection according eq. (2) with $\Delta = 1.0$

6. 6 partitions, reflection according eq. (2) with $\Delta = 1.0$
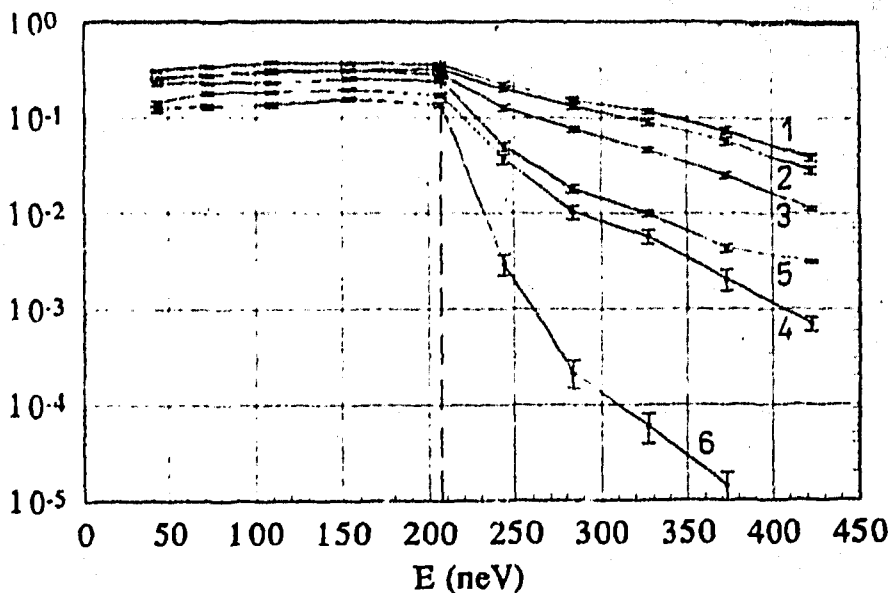
Fig.12 Energy dependence of neutron transmission through the filtering configuration of fig.2c, $a = b = c = 6cm$, $d = 0$, $e = 3cm$ neutron loss coefficient of the inside surface $\eta = 5 \cdot 10^{-4}$, $\alpha = 0.5$, with different numbers of partitions and different degrees of inner surface roughness; the entrance of the filter is connected to the neutron guide with a cross section $6 \times 6cm^2$, length $6m$ and neutron surface reflection law according to eq. (3) with parameters $\sigma = 30$ Å, $T = 250$Å; the exit of the filter is connected to the irradiation chamber with a return probability $\alpha = 0.5$

1. 3 partitions, mirror reflections

2. 3 partitions, reflection according eq. (2) with $\Delta = 0.25$

3. 3 partitions, reflection according eq. (2) with $\Delta = 1.0$

4. 6 partitions, mirror reflections

5. 6 partitions, reflection according eq. (2) with $\Delta = 0.25$

6. 6 partitions, reflection according eq. (2) with $\Delta = 1.0$

surface properties on neutron filtering for the device of fig.2a, and fig.5 shows the dependence of filtering on the size of device. The influence of inner neutron guide length is seen in fig.6.

In reality irradiation chambers are usually connected to the exit of the filters so that a significant portion of UCN return to the filter volume, and there is some probability that some of them will re-enter the irradiation chamber. In the calculations this was taken into account by the random choice of coordinates and angles (cosine law) of return of neutrons into the filter from the exit window with probability α. Fig.7 illustrates this effect. In this and further calculations the additional appearances of UCN at the exit of the device are taken into account additively in the "transmission probability" - normalization is performed to one neutron at the entrance to the device.

The transport neutron guide at the entrance of the filter also has the ability to return neutrons which leave the filter through the entrance window and re-enter the filter. Fig.8 shows the probability of a neutron returning from neutron guides of different lengths. The effect of this returning on the filtering characteristics is shown in fig.9. For simulation of UCN transport in these cases the normalization was changed again – the transmission coefficient was the ratio of UCN fluxes at the exit chamber with and without the filter.

As is seen from fig.5, better filtering characteristics of the device in fig.2a are achieved by increasing the size of the chamber. The reason for this is the increase in the number of neutron collisions inside the chamber before leaving the chamber. But the same effect can be achieved by increasing the internal surface area without increasing the volume by covering of surface with ribs. The effect of additional ribs on filtering is shown in fig.10. The presence of surface ribs was not simulated exactly but merely by adding several additional chance reflections of neutrons with the surface at the same surface coordinates.

Figs.11 and 12 show the filtering characteristics of the simple devices of figs.2b and 2c. The parameters of these devices (lengths of intervals between partitions, and lengths and heights of inclined partitions) were optimal choices from different variants. As is seen, the filtering properties of the device of the type shown in fig. 2b are very sensitive to the the surface roughness parameters – the filtering characteristics are satisfactory for a very rough surface, which is as difficult to realize and

control as a very smooth one. The filters of fig.2c are not so dependent on surface roughness. The common property of the filters of fig.2b and 2c is their simplicity of construction and satisfactory filtering properties for a large number of elements, but they have significant losses of useful sub-barrier UCN.

Figs.13-16 show the influence of different parameters on the filtering characteristics of the filter described by the geometry of fig.2d, and fig.17 comprises the comparative curves for different devices. The reason for different behaviours of the transmission curves can be seen partly from figs.18-20, where the distribution of the number of neutron reflections is shown for the devices of fig.2a and 2d. The difference in these distributions is based on the fact that there is no chance a neutron can escape from the exit window of the filter of fig.2d without the number of reflections being less than approximately twice the number of elements of the device – in sharp contrast to the distributions for the fig.2a filter in which there is always some probability of reaching the exit after only two reflections inside the chamber. The filters of fig. 2d have the best filtering properties but seem to require high precision in construction and geometric fitting of the elements to each other. We have not yet investigated the sensitivity of the parameters of the filter in fig.2d to distortions of the geometry from the ideal half cylinder and to errors in fitting the elements of the device.

The quantitative characteristics of different filters can be elucidated better if they are compared with applications to some particular experiment, for example, the measurement of the capture probability of UCN by the wall with boundary energy E_b at the sub-barrier reflection. In this case the presence of super-barrier neutrons, with their high probability of propagation into the wall, will cause misinterpretation of the measured value.

Two integral parameters may be introduced to characterize the quality of the filter: integral transmission K of useful sub-barrier UCN

$$K = \int_0^{E_b} J(E + \Delta E) \cdot P(E) \cdot dE \bigg/ \int_0^{E_b} J(E) \cdot dE, \qquad (15)$$

and the filtering coefficient

$$D = \int\limits_{E_b}^{\infty} J(E + \Delta E) \cdot P(E) \cdot T(E) \cdot dE \bigg/ \int\limits_{0}^{E_b} J(E + \Delta E) \cdot P(E) \cdot dE. \quad (16)$$

The K value shows the relative quantity of sub-barrier UCN transmitted through the filter (boundary energy of **the irradiated surface** is E_b), $\Delta E = mgh$ is the gravitational deceleration of neutrons for filters in which exit window is higher than the entrance one by an altitude h (fig.1a). $J(E)$ is the incoming neutron spectrum, $P(E)$ is the transmission of neutrons with an energy E, $T(E)$ is the averaged over isotropic angular distribution probability of a super-barrier neutron penetrating the bulk of the wall of the irradiated surface.

The D value shows the integral probability of propagation of the admixture of super-barrier neutrons into the wall, $T(E)$ is integrated over the solid angle probability of propagation into the wall of super-barrier neutrons with energy E.

The Table I shows the values of K and D for different filters, characterized by the curves of fig.17 for the boundary energy of the irradiated surface $E_b = 204 neV$.

Table I

Filter (No. of curve)	1	2	3	4	5
K (ILL spectrum)	0.33	0.347	0.26	0.61	0.46
D (ILL spectrum)	2.0 E-3	8.5 E-4	3.8 E-4	5.7 E-4	4.09 E-5
K (PINP spectrum)	0.34	0.34	0.28	0.56	0.457
D (PINP spectrum)	9.2 E-4	4.14 E-4	1.7 E-4	2.95 E-4	1.98 E-5

The next Table shows the values of K and D for different filters, characterized by the curves of fig.17 for the boundary energy of the irradiated surface $E_b = 242 neV$, which corresponds to beryllium.
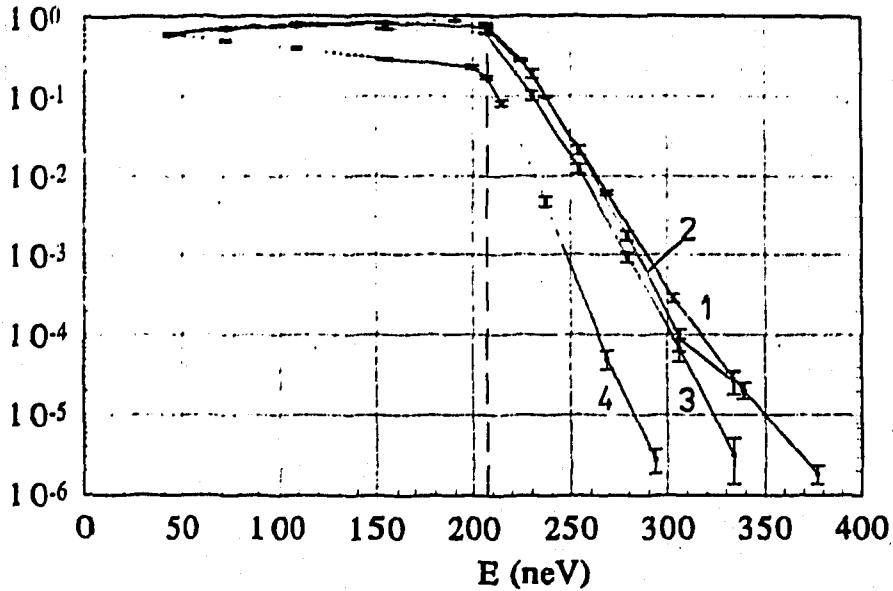
Fig.13 Energy dependence of neutron transmission through the filtering configuration of fig.2d, with dimensions $a = b = 6cm$, number of sections $n = 21$, for different degrees of surface roughness and a neutron loss coefficient η of the inside surface:

1. ideal specular reflection, $\eta = 0$.

2. the same, but $\eta = 5 \cdot 10^{-4}$,

3. $\eta = 5 \cdot 10^{-4}$, neutron surface reflection law according to eq. (3) with parameters $\sigma = 30$ Å, $T = 50$Å,

4. $\eta = 5 \cdot 10^{-4}$, neutron surface reflection law according to eq. (3) with parameters $\sigma = 30$ Å, $T = 250$Å,
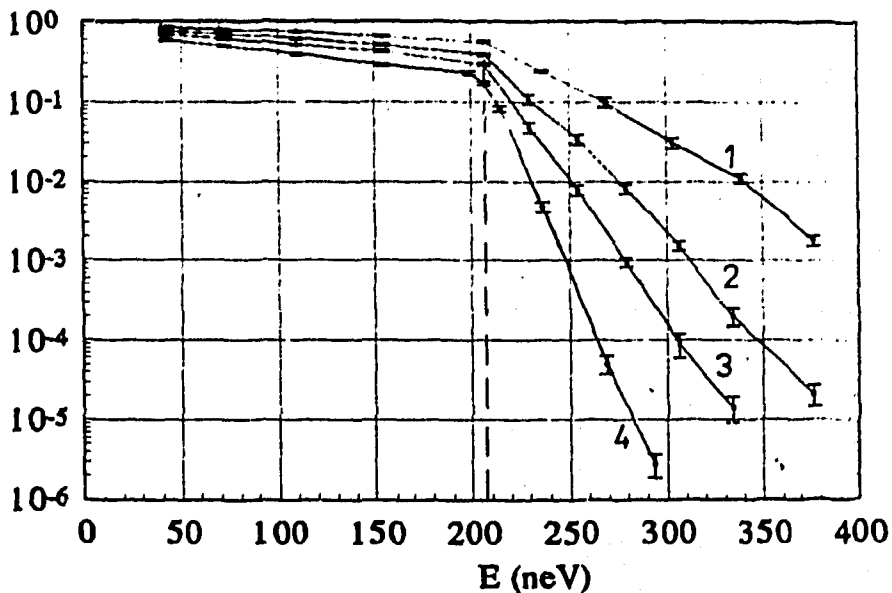
Fig.14 Energy dependence of neutron transmission through the filtering configuration of fig.2d, with different numbers of elements n, neutron loss coefficient of the inside surface $\eta = 5 \cdot 10^{-4}$, and a neutron surface reflection law according to eq. (3) with parameters $\sigma = 30$ Å, $T = 250$Å,

1. $n = 5$

2. $n = 9$

3. $n = 13$

4. $n = 21$
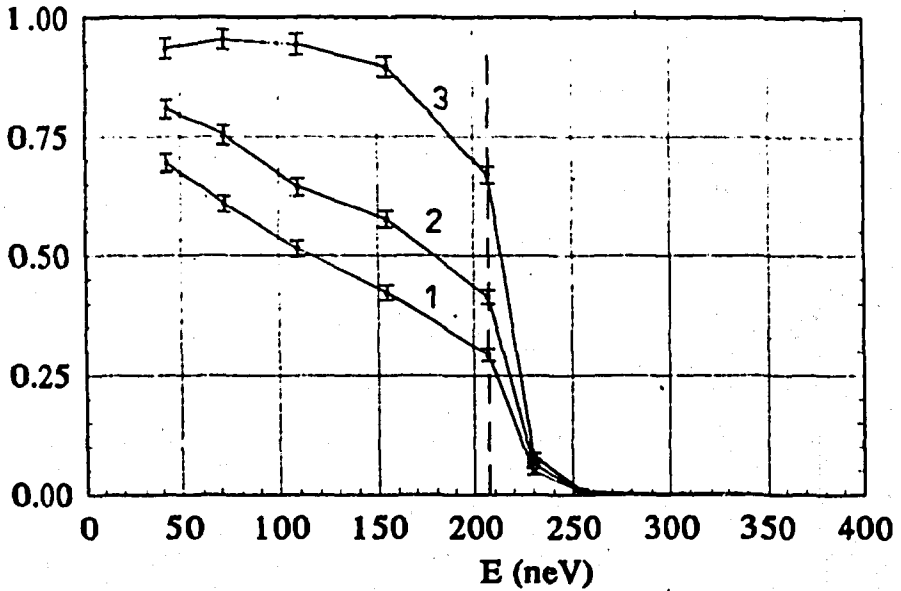
Fig.15 Energy dependence of neutron transmission through the filtering configuration of fig.2d, with dimensions $a = b = 6cm$, $n = 13$, neutron loss coefficient of the inside surface $\eta = 5 \cdot 10^{-4}$, reflection law according to eq. (3) with $\sigma = 30$Å, $T = 250$Å, for different probabilities α of UCN return from the exit window of device:

1. $\alpha = 0$

2. $\alpha = 0.5$

3. $\alpha = 0.95$
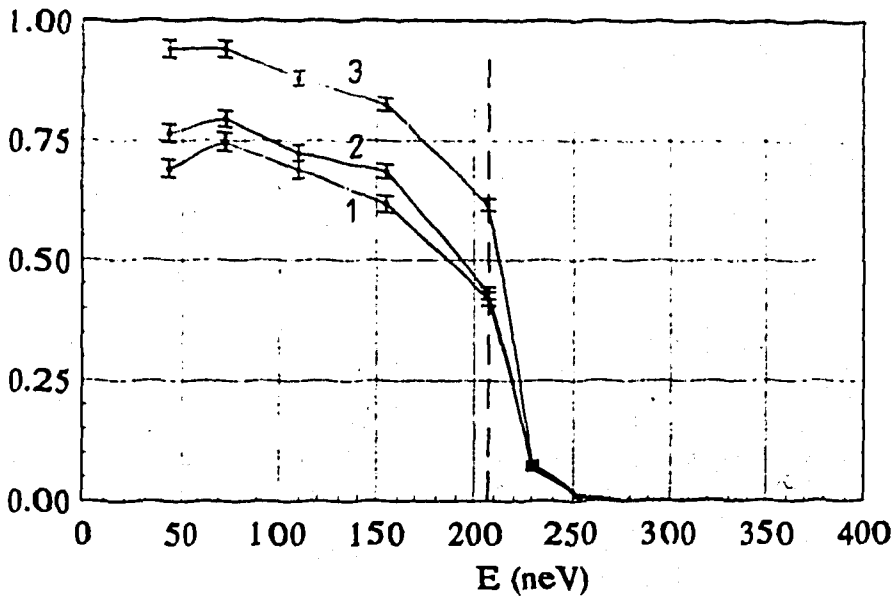
Fig.16 The same as in fig.15, but the entrance of the filter is connected to the neutron guide with a cross section $6 \times 6cm^2$, length $6m$ and a neutron surface reflection law according to eq. (3) with parameters $\sigma = 30$ Å, $T = 250$Å.
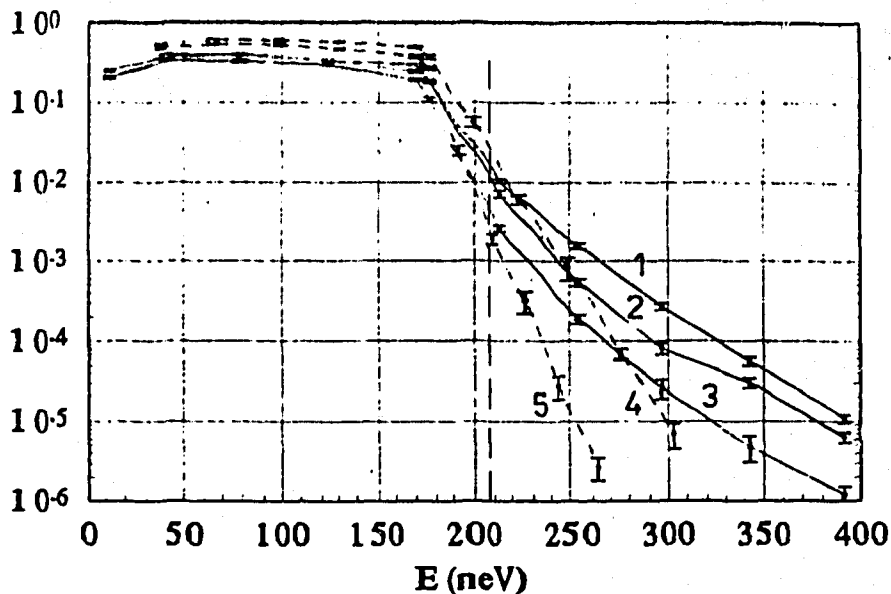
Fig.17 Comparative curves for energy dependence of neutron transmission through different filtering configurations having the same external conditions: probability of UCN return from the exit window of device $\alpha = 0.5$, the entrance of the filter is connected to the neutron guide with a cross section $6 \times 6 cm^2$, length $6m$ and neutron surface reflection law according to eq. (3) with parameters $\sigma = 30$ Å, $T = 250$Å,

1. filter of fig.2a configuration with dimensions $a = 40cm$, $b = 40cm$, $c = 100cm$, neutron loss coefficient of the inside surface $\eta = 5 \cdot 10^{-4}$, inner neutron guides with a length of $90cm$ have a reflection law according to eq. (3) with $\sigma = 30$Å, $T = 250$Å; the inside surface has a reflection law according to eq. (2) with $\Delta = 0.25$

2. configuration of fig.2a, with dimensions $a = 15cm$, $b = 40cm$, $c = 50cm$, neutron loss coefficient of the inside surface $\eta = 5 \cdot 10^{-4}$, inner neutron guides with a length $45cm$ have a reflection law according to eq. (3) with $\sigma = 30$Å, $T = 250$Å; the inside surface has a reflection law according to eq. (2) with $\Delta = 0.25$, with ribs covering the inner surface, increasing its area 2.5 times

3. the same with ribs covering the inner surface, increasing its area 5 times

25

4. configuration of fig.2d, with dimensions $a = b = 6cm$, $n = 13$, neutron loss coefficient of the inner surface $\eta = 5 \cdot 10^{-4}$, reflection law according to eq. (3) with $\sigma = 30\text{Å}$, $T = 250\text{Å}$

5. the same with the number of elements $n = 21$

Curves 4 and 5 were calculated for the case when a vertical neutron guide of the height 30 cm was connected to the exit of the filter to satisfy the same spectral conditions as in curves 1-3.
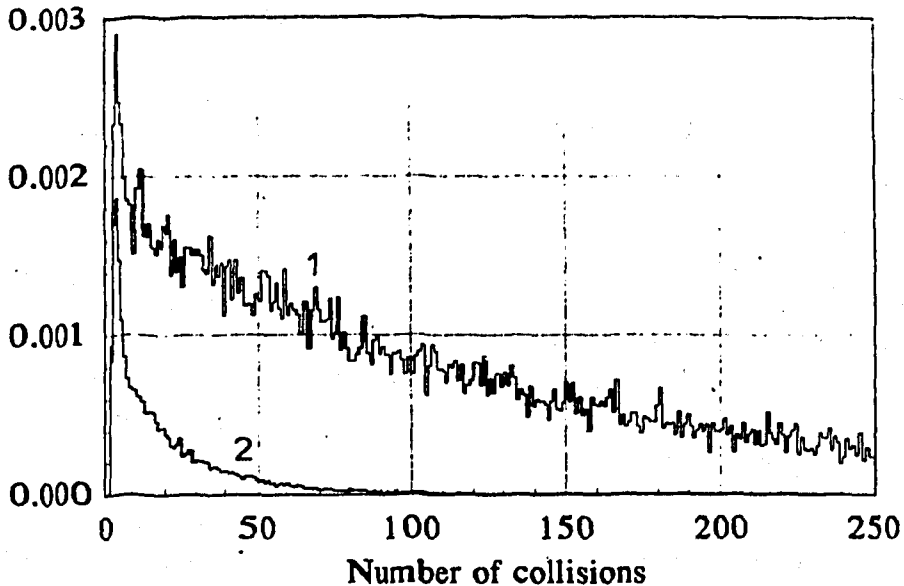
Fig.18 Distributions of the number of neutron collisions inside the device of fig. 2a with dimensions $a = 15cm$, $b = 40cm$, $c = 50cm$, neutron loss coefficient of the inside surface $\eta = 5 \cdot 10^{-4}$; inner neutron guides with a length $l = 45cm$ have a reflection law according to eq. (3) with $\sigma = 30\text{Å}$, $T = 250\text{Å}$; the inner surface has a reflection law according to eq. (2) with $\Delta = 0.25$, for different neutron velocities v:

1. $v = 6.0 m/s$

2. $v = 7.0 m/s$

26
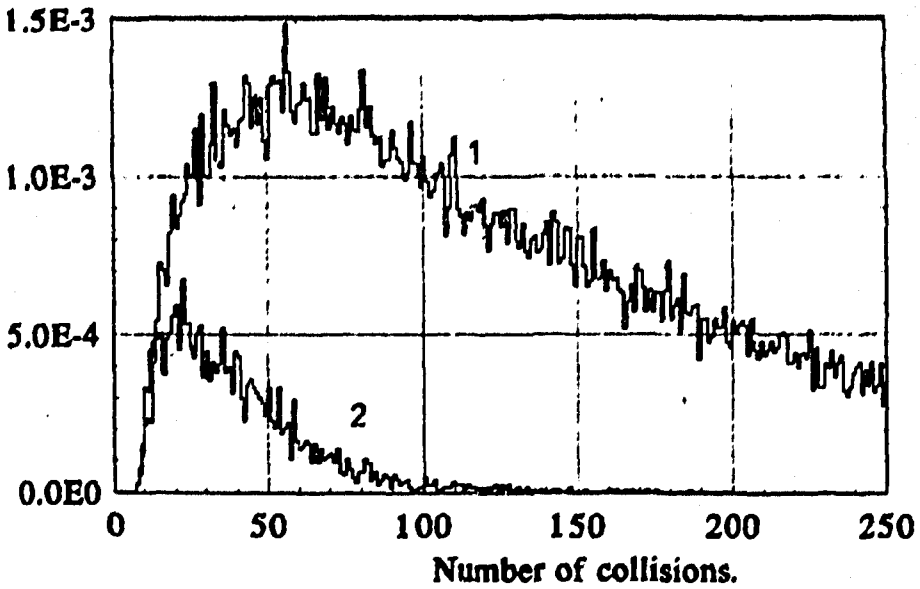
Fig.19 The same as in fig.18, but accounting for collisions in the inner neutron guides.
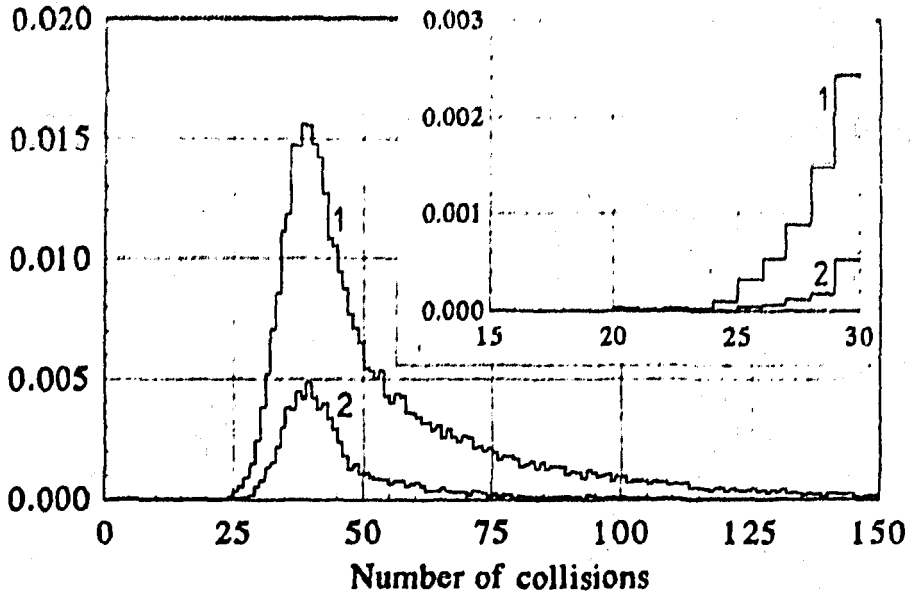
Fig.20 Distribution of the number of neutron collisions inside the device of fig. 2d with dimensions $a = b = 6cm$, neutron loss coefficient of the inner surface $\eta = 5 \cdot 10^{-4}$; inner surface has a reflection law according to eq. (3) with $\sigma = 30\text{Å}$, $T = 250\text{Å}$, number of elements $n = 13$, for different neutron velocities v:

1. $v = 6.0m/s$

2. $v = 6.6m/s$

Table II

Filter (No. of curve)	1	2	3	4	5
K (ILL spectrum)	0.20	0.21	0.16	0.37	0.28
D (ILL spectrum)	4.5 E-4	1.6 E-4	6.0 E-5	3.07 E-5	5.3 E-7
K (PINP spectrum)	0.214	0.26	0.21	0.43	0.346
D (PINP spectrum)	2.14 E-4	7.97 E-5	2.7 E-5	1.57 E-5	2.5 E-7

Consider a particular experiment, in which the presence of the admixture of super-barrier neutrons is detrimental. It can be seen from the tables that for the search for anomalous propagation of sub-barrier UCN into the the bulk of the wall with boundary energy $E_b = 204neV$ on the level 10^{-5} none of the filters characterized by the curves of fig.17 is applicable. For $E_b = 240neV$ only the filter of curve 5 fits the requirements of the experiment.

4   Conclusion

The goal of the Monte Carlo simulations of UCN transmission, performed for four different types of spectral UCN filters, was to outline quantitatively the level of presence of super-barrier neutrons in experiments with the use of these filters and to give their comparative characteristics. It was shown that serious precautions have to be made to achieve a significant level of removal of superbarrier neutrons from the UCN spectrum, and any particular experiment, in which these neutrons play a detrimental role must be carefully simulated beforehand.

References

[1] A.Steyerl et al., Phys.Lett. A116 (1986) 269

[2] I.S.Altarev, Dissertation, LNPI, Leningrad, 1986.

[3] J.M.Pendlebury, Annu. Rev. Nucl. Part. Sci., 43 (1993) 687

[4] V.P.Alfimenkov et al., Pis'ma ZETF, 55 (1992) 92; JETP Lett. 55 (1992) 84

[5] V.P.Alfimenkov et al. LNPI Preprint No.1729, Gatchina, Russia (1991);

[6] A.V.Strelkov and M.Hetzelt, ZETF, 74 (1978) 23

[7] M.I.Novopoltsev and Yu.N.Pokotilovski, JINR Commun. P3-85-843 (1985); M.I.Novopoltsev et al. Z.Phys. B70 (1988) 199

[8] A.Steyerl, Z.Phys.254 (1972) 169

[9] A.Steyerl, Nucl. Instr. Meth., 101 (1972) 295

[10] F.G.Bass and I.M.Fuks, "Scattering of Waves on a Statistically Non-flat Surface", Nauka, Moscow, 1972, ch.VII (in Russian).